Developmental Biology 408 (2015) 66–78

Contents lists available at ScienceDirect

Developmental Biology

journal homepage: www.elsevier.com/locate/developmentalbiology

Distinct modes of mitotic spindle orientation align cells in the dorsal midline of ascidian embryos

Takefumi Negishi [1], Hitoyoshi Yasuo *

Sorbonne Universités, Université Pierre et Marie Curie, Univ Paris 06, CNRS, Laboratoire de Biologie du Développement de Villefranche-sur-Mer, Observatoire Océanologique, 06230 Villefranche-sur-Mer, France

ARTICLE INFO

Article history:
Received 10 August 2015
Received in revised form
25 September 2015
Accepted 25 September 2015
Available online 9 October 2015

ABSTRACT

The orientation of cell division can have important consequences on the choice of cell fates adopted by each daughter cell as well as on the architecture of the tissue within which the dividing cell resides. We have studied in detail the oriented cell divisions that take place in the dorsal midline of the ascidian embryo. The dorsal midline cells of the ascidian embryo emerge following an asymmetric cell division oriented along the animal–vegetal (A–V) axis. This division generates the NN (Notochord–Neural) cell at the margin and the E (Endoderm) cell more vegetally. Deviating from the default mode of cell division, these sister cells divide again along the A–V axis to generate a column of four cells. We describe these cell divisions in detail. We show that the NN cell mitotic spindle rotates 90° to align along the A–V axis while the E cell spindle forms directly along the axis following the asymmetric migration of its centrosomes. We combine live imaging, embryo manipulations and pharmacological modulation of cytoskeletal elements to address the mechanisms underlying these distinct subcellular behaviours. Our evidence suggests that, in E cells, aster asymmetry together with the E cell shape contribute to the asymmetric centrosome migration. In NN cells, an intrinsic cytoplasmic polarisation of the cell results in the accumulation of dynein to the animal pole side. Our data support a model in which a dynein-dependent directional cytoplasmic pulling force may be responsible for the NN cell spindle rotation.

1. Introduction

The orientation of the cell division axis has important consequences for tissue architecture and cell fate. The cell division axis is defined by the orientation of the mitotic spindle, with the cleavage furrow always forming at right angles to the spindle (reviewed in Conrad and Rappaport, 1981). According to Sachs's rule, which was originally proposed based on his studies on plant cells, each new cell division plane intersects the preceding plane at a right angle so that the "default" orientation of a spindle would be 90° to the previous spindle (reviewed in Wilson, 1925; Strome, 1993). The 90° default orientation can be explained by the movements of the duplicated centrosomes, which migrate 90° in opposite directions around the nucleus and serve as the asters of the next mitotic spindle. Hertwig formulated another important rule stating that spindles align with longest axis of the cell, such that spindle orientation can be controlled by cell shape. Minc et al. (2011) further refined Hertwig's rule by proposing a computational model that fully predicts the orientation of a mitotic spindle of sea urchin eggs imposed into various shapes. The key element of this computational model is the assumption that a cytoplasmic pulling force generated on the spindle pole by each microtubule is proportional to its length, as initially proposed by Hamaguchi and Hiramoto (1986). However, *in vivo* evidence for the presence of such a pulling force in the context of cell shape-dependent spindle orientation is lacking. Most of our current knowledge on the molecular control of spindle orientation in metazoans is based on asymmetric cell divisions of highly polarised cells such as the *Drosophila* neuroblasts (NBs) and sensory organ precursors (SOPs) and the *C. elegans* zygote (reviewed in Morin and Bellaïche, 2011). In these systems, distinct polarising cues converge on cortical NuMA proteins. The NuMA family of proteins regulate the activity of the dynein/dynactin motor complex to exert a pulling force on astral microtubules from the cell cortex (Morin and Bellaïche, 2011). Importantly, the cortical NuMA-based mechanism is likely to be evolutionary-conserved since it also operates in chick neuroepithelium (Peyre et al., 2011), mouse embryonic skin progenitors (Lechler and Fuchs, 2005) and mammalian cell culture systems (Zheng et al., 2010; Kiyomitsu and Cheeseman, 2012). However, it is not yet clear whether the NuMA-based system is applicable to all oriented cell divisions.

* Corresponding author. Fax: +33 4 93 76 39 82.
E-mail address: yasuo@obs-vlfr.fr (H. Yasuo).
[1] Current address: National Institute for Basic Biology, Division of Morphogenesis, Nishigonaka 38, Myodaiji, Okazaki 444-8585 Aichi, Japan.

http://dx.doi.org/10.1016/j.ydbio.2015.09.019
0012-1606/

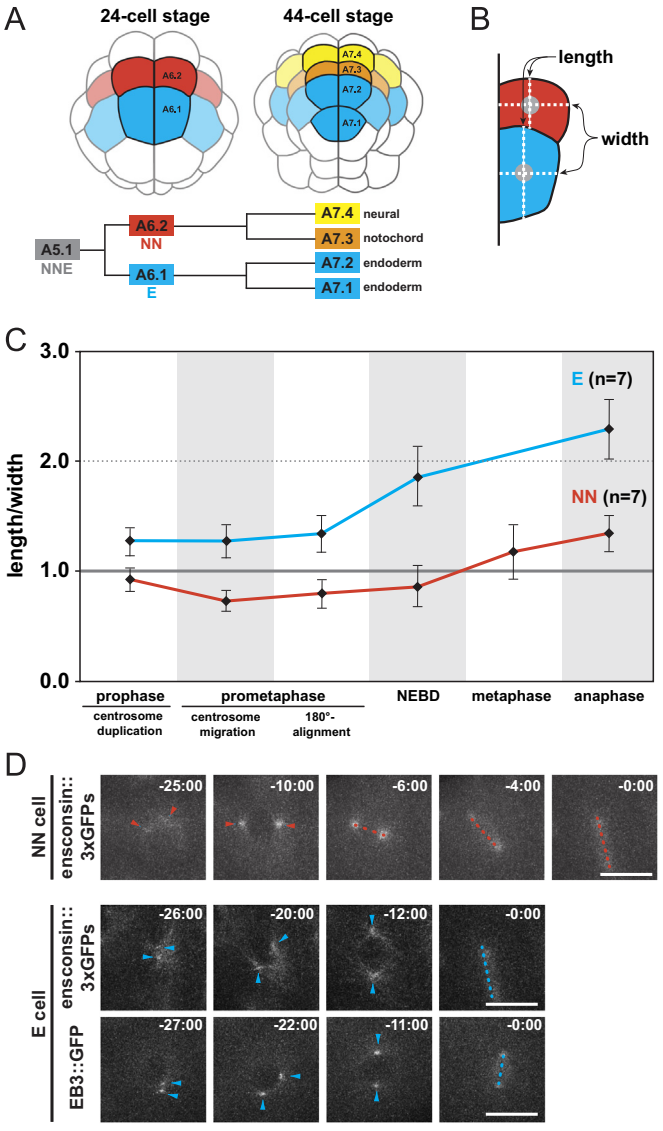

Fig. 1. Oriented cell division of the medial NN and E cells. (A) Drawings of the 24- and 44-cell stage embryos highlighting the cell lineage of the medial pair of NNE cells (A5.1 cells). Embryos are in vegetal pole view with dorsal side up. NNE cell divides into one Notochord/Neural mother cell (NN cell/A6.2, in red) and one Endodermal precursor (E cell/A6.1, in blue) at 24-cell stage. The division axis is parallel to the "meridian" line connecting the animal and vegetal poles. For simplicity, this geodesic is referred to as A–V axis in the text. These two daughter cells then divide again along the A–V axis to generate one neural precursor (A7.4, in yellow), one notochord precursor (A7.3, in orange) and two endoderm precursors (A7.2 and A7.1, in blue) at the 44-cell stage. (B) Schematic drawing representing how the length and width of NN and E cells were measured (dashed lines). Grey circles and black vertical line represent nuclei and the embryonic midline, respectively. Animal pole side is at the top and embryo midline on the left. (C) Measurement of the length/width ratio of NN and E cells during their cell cycle. The temporal changes to the length/width measurements of NN cells are represented by a red line and E cells by a blue line. "180°-alignment" indicates the time point at which the centrosomes become aligned 180° around the nucleus in both cells. Error bars indicate the standard deviation. (D) Centrosome and spindle dynamics in NN and E cells. Upper panel: selected frames from a confocal 4D image set of an NN cell in an ensconsin::3xGFP-expressing embryo. Bottom panel: selected frames from confocal 4D image sets of E cells in (upper) ensconsin::3xGFP- and (lower) EB3::GFP-expressing embryos. Each image is a max intensity projection of selected z-sections. Arrowheads indicate centrosomes and dotted lines correspond to the spindle axis, in red for NN and blue for E cells. Animal pole side is up and embryo midline on the right. Time is indicated as minutes:seconds with 0:00 corresponding to the onset of anaphase. Scale bars are 20 μm.

The embryogenesis of many invertebrates proceeds with an invariant cell division pattern (Wilson, 1925; Freeman, 1983). An invariant cell division pattern implies a precise control of cell division orientation and timing. In many animal groups, the mechanisms controlling these precise cell division patterns have not been addressed. In this study, we use ascidian embryos, which develop with an invariant bilateral holoblastic cleavage pattern (Conklin, 1905), as a model to explore oriented cell divisions. Ascidians are invertebrate chordates of the phylum Tunicata, a sister group of the vertebrates (Delsuc et al., 2006; Vienne and Pantarotti, 2006; Satoh et al. 2014). The blastula fate maps of ascidians and vertebrates reveal a high degree of topological similarity and ultimately give rise to tadpole larvae with a central notochord and dorsal hollow nervous system (Lemaire et al., 2008). In this study, we focus on two oriented cell divisions that take place in the dorsal midline of ascidian blastula stage embryos (Fig. 1A). These oriented cell divisions occur in a sister cell pair, named NN (Notochord/Neural) and E (Endoderm) cells. Their mother cell, the NNE cell (Notochord/Neural/Endoderm), divides along the animal–vegetal (A–V) axis to generate one NN cell and one E cell. Contrary to Sachs's rule, these sister cells then divide again along the A–V axis to form a column of four cells on the dorsal side of the 44-cell "blastula" stage embryo (Fig. 1A). The molecular mechanisms that determine the differential fates of daughter cells following each of these asymmetric divisions are well documented (Hudson et al., 2013; Takatori et al., 2010; Kim et al., 2007; Minokawa et al., 2001; Picco et al., 2007). Here we provide a detailed description of the oriented cell division of NN and E cells along the A–V axis and present our evidence showing that distinct mechanisms govern spindle orientation in these two cell types.

2. Results

2.1. Oriented cell divisions of the medial NN and E cells

All experiments described in this study were conducted using the ascidian, *Phallusia mammillata*. *Phallusia* embryos are transparent and injected mRNA is efficiently translated in eggs, thus enabling the visualisation of tagged proteins and subcellular structures in living eggs and embryos (Prodon et al., 2010). Importantly, all cell divisions up to the gastrula stage take place within the planar plane. As described above, contrary to Sachs's rule, NN and E cells both divide along the A–V axis as their mother cell (NNE) did. We addressed whether Hertwig's rule could instead be implicated in the NN and E cell divisions. To do this, we conducted live-imaging of embryos in which microtubules and cell membranes were labelled with ensconsin fused with three GFPs in tandem (ensconsin::3xGFP) (von Dassow et al., 2009; Negishi et al., 2013) and FM4-64 (Prodon et al., 2010), respectively. NN and E cells are quadrilateral (=tetragon) with one side corresponding to the embryonic midline (Fig. 1B). To describe length, we measured the line that is parallel to the embryonic midline and crosses the centre of the nucleus or of the spindle (Fig. 1B). For the width, the line that is perpendicular to the length and crosses the centre of the nucleus or spindle was measured (Fig. 1B). During prophase and prometaphase, the length/width ratio of NN cells remains below 1.0, but increases during metaphase to reach 1.3 ± 0.16 by anaphase ($n=7$ cells) (Fig. 1C, red line). The E cell on the other hand is elongated throughout the entire cell cycle (Fig. 1C, blue line). Thus, for both NN and E cells, the cell division axis corresponds to the final long axis of the cell.

While both NN and E cells divide along the long axis of the cell, our observations of centrosome and spindle dynamics revealed that their spindles align via distinct mechanisms (Fig. 1D; Movie 1). In the NN cell, the duplicated centrosomes are located on the

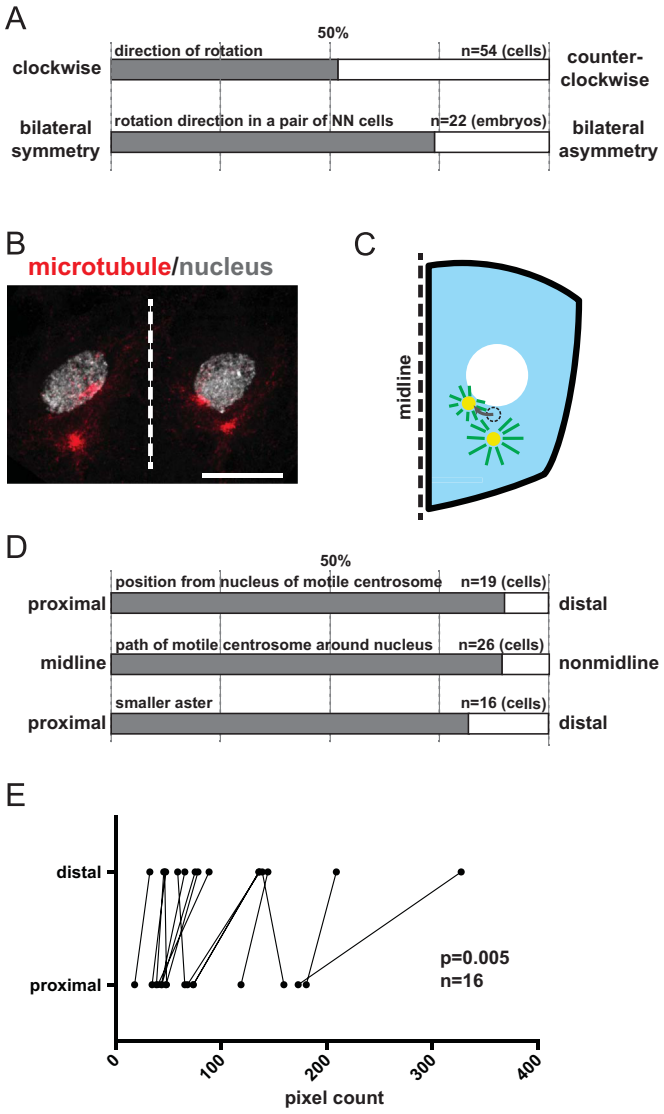

Fig. 2. Description of oriented cell divisions of NN and E cells. (A) Description of the spindle rotation in NN cells. Upper, the direction of spindle rotation in individual NN cells (clockwise or counter-clockwise); lower, the direction of spindle rotation of NN cell pairs in single embryos ("bilateral symmetry", one clockwise and the other anti-clockwise; "bilateral asymmetry", both clockwise or both counter-clockwise). (B) Differential aster size in E cells. The image shows a pair of E cells at prometaphase immunostained for microtubules and counterstained for nucleus (DAPI). Animal pole side is up and vertical dotted line represents the embryonic midline. The image is a max intensity projection of selected z-sections. Scale bar is 20 μm. (C) Schematic drawing of an E cell highlighting characteristic behaviours of centrosomes as described in (D). Animal pole side is at the top and embryo midline on the left. (D) Description of the asymmetric centrosome migration in E cells. Top, the proximal centrosome relative to the nucleus position tends to become motile (89.5%); middle, the motile centrosome tends to take the route on the embryonic midline side (88.5%); bottom, the proximal centrosome tends to exhibit a smaller aster (80.0%). Data shown in the top and middle bars was based on analysis of 4D image sets. Data in the lower bar was based on analysis of immunostained embryos as show in (B). (E) Graph showing a differential aster size between the distal and proximal centrosome pair. A set of 16 centrosome pairs was analysed as described in the Materials and Methods. $p=0.005$ (by paired t-test).

animal pole side of the cell. During prophase, the centrosomes migrate 90° in opposite directions within the plane of the apical contour (Fig. 1D). During metaphase, the mitotic spindle undergoes a 90° rotation to align along the A–V axis. This rotation can also be observed with DIC microscopy (Movie 2). From spindle formation to A–V alignment takes 7.2 ($\pm$ 1.1) minutes ($n=12$). The direction of spindle rotation is not biased with both clockwise and counter-clockwise directions observed equally ($n=54$) (Fig. 2A). However, within individual embryos, the mitotic spindles of NN cell pairs tend to rotate with bilateral symmetry (72.7%) (Fig. 2A). The E cell exhibits a different sequence of centrosome/aster movements. In E cells, following centrosome duplication, one centrosome becomes preferentially migratory and moves approximately 180° around the nuclear envelope such that when the mitotic spindle forms it is directly aligned with the A–V axis (Fig. 1D; Movie 1). From centrosome duplication to A–V spindle formation takes 14.4 ($\pm$ 2.5) minutes ($n=18$).

Supplementary material related to this article can be found online at http://dx.doi.org/10.1016/j.ydbio.2015.09.019.

In summary, the spindles in NN and E cells align along the long axis of the cells by distinct mechanisms. In the following sections, we describe in further detail, first, the centrosome positioning mechanism in E cells and, subsequently, the spindle rotation in NN cells.

2.2. Correlation between asymmetric centrosome migration of the E cell and cell shape

Differential migratory behaviour of duplicated centrosomes has been reported to underlie the oriented cell divisions of *Drosophila* stem cells, namely neuroblasts and male germ line stem cells (Rebollo et al., 2009; Yamashita et al., 2003). In these stem cell systems, the duplicated centrosomes exhibit differential microtubule organising (MTOC) activities with the immobile centrosome showing a more robust astral microtubule array (Rebollo et al., 2009; Yamashita et al., 2007). When the centrosome of the E cell first duplicates, the duplicated centrosomes align along the A–V axis and, in a majority of cases (89.5%), the centrosome proximal to the nucleus starts to migrate away from its distally-positioned counterpart (Figs. 1D and 2C, D; Movie 1). The motile centrosome migrates around the nucleus, preferentially taking the route facing to the embryonic midline (88.5%) (Figs. 1D and 2C, D; Movie 1). Finally, we observed a difference in size between proximal and distal asters. Using images of embryos immunostained for α-tubulin, we counted the number of pixels in the proximal and distal asters of E cells and found that the distal aster was larger in size to the proximal aster (in 80.0% of cases) (Fig. 2B, D and E). This could indicate an asymmetry in MTOC activity or differential microtubule stability between the two asters.

The degree of asymmetry in E cell centrosome migration appeared variable (Fig. 3A). To express this variation quantitatively, we measured the angle between the position of the newly duplicated centrosomes and the position of the distal-most centrosome when migration was complete (centrosomes 180° apart) (Fig. 3C). We refer to this angle as the centrosome migration angle (θ) (Fig. 3C). In 10/18 of E cells, the centrosome migration angle falls between 150° and 180°, which we classed as 'asymmetric' (Fig. 3A, D). However, the remaining E cells analysed exhibited either 'moderate asymmetry' ($120° < \theta < 150°$; 4/18) or 'symmetry' ($90° < \theta < 120°$; 4/18) in their centrosome migration. Even in the cases where centrosome migration was classed as 'moderate asymmetry' or 'symmetry', the spindle ultimately aligns with the A–V axis (Fig. 3A). This adjustment takes place either via rotation of the centrosome-nucleus complex or via spindle rotation.

We first addressed whether the E cell asymmetric centrosome migration was an intrinsic property of E cells. Individual E cells were isolated at the 24-cell stage from embryos expressing ensconsin::3xGFP to observe centrosome dynamics. In isolated E cells, we did not observe any centrosome migration classed as 'asymmetric' (0/9), suggesting that contact with other cells may be required for asymmetric centrosome migration (Fig. 3B and D). In *Drosophila* male germ line stem cells (GSCs) that exhibit a similar asymmetric centrosome migration, an adherence junction-mediated contact site with a stem cell niche defines the position of the

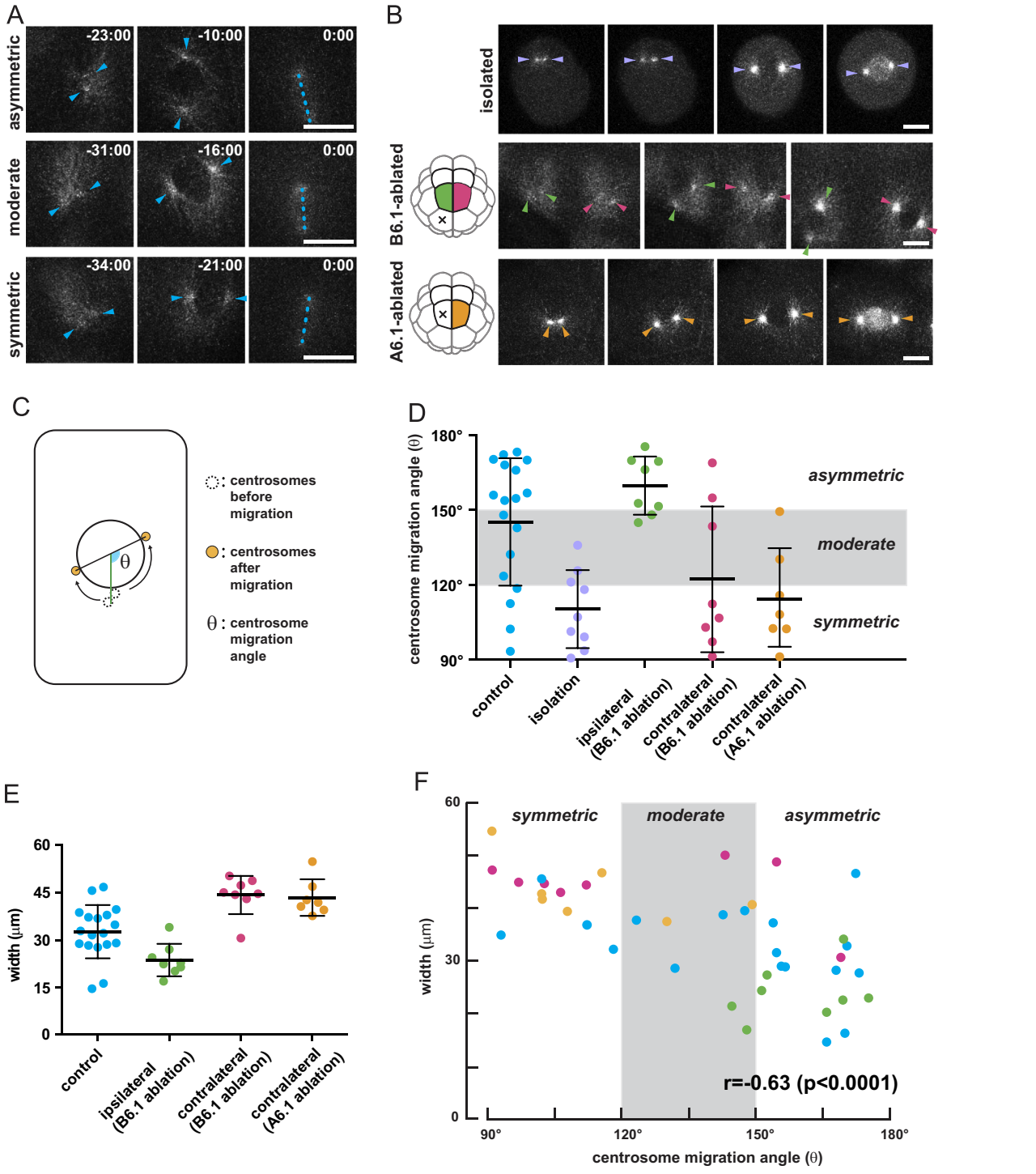

Fig. 3. Correlation between cell shape and asymmetric centrosome migration in E cells. (A and B) Panels show selected frames from 4D image stacks of embryos expressing ensconsin::3xGFP. Each frame is a max intensity z-projection of selected confocal planes. Scale bars are 20 μm. (A) Variation in asymmetric centrosome migration. Blue arrowheads and dotted lines indicate centrosomes and spindle axis, respectively. Time is indicated as minutes:seconds with 0:00 corresponding to the time when the spindle forms. (B) E centrosome dynamics in manipulated embryos. Top row, isolated E cell; middle row, E cell pairs in embryos in which one B6.1 cell is ablated; bottom row, E cell whose contralateral pair was ablated. Arrowheads indicate the centrosomes, following the colour code of the 24-cell embryo drawings on the left, purple for isolated E cells. Diagonal crosses in the drawings indicate ablated cells. (C) Schematic drawing of the "centrosome migration angle (θ)", measured to quantify the degree of asymmetry in centrosome migration under the various conditions. Yellow filled circles represent centrosomes at the end of migration while dotted circles indicate centrosomes at the onset of migration. Large open circle represents the nucleus. The angle (θ) between the green and black lines is the centrosome migration angle. (D) Graph showing the variation in the asymmetry of E cell centrosome migration under the conditions listed in the X-axis. Each coloured circle represents the centrosome migration angle (θ) for each E cell using the same colour code as the arrowheads in (A) and (B). Bars represent means and SDs. (E) Graph showing the variation in the width of E cells under the conditions listed in the X-axis. Bars represent means and SDs. (F) Plot showing a negative correlation between the centrosome migration angle (θ) and the width of E cells (μm). A coloured circle represents each of the E cells measured in (D). The correlation coefficient (r) is -0.63 ($p < 0.0001$) (Pearson correlation using GraphPad Prism 6 software).

immotile centrosome (Yamashita et al., 2003). The symmetrical centrosome migration observed in isolated E cells might thus be due to a loss of contact with specific neighbouring cells. The B6.1 cell would be a good candidate for a cell that provides such a contact site since it is positioned on the vegetal side of the E cell, where the immotile centrosome is predominantly observed (Fig. 3B, middle panels). In order to test whether the asymmetric centrosome migration requires contact with B6.1, we ablated one B6.1 cell from early 24-cell stage embryos and observed centrosome dynamics (ensconsin::3xGFP) in the E cell pair (Fig. 3B and D). To our surprise, in the E cell that no longer had contact with B6.1, asymmetric centrosome migration was not lost, with 6/8 cells classed as asymmetric (green cell in Fig. 3B and D). On the other hand, in the E cell on the non-ablated (=contralateral) side, that is, in the E cell that retained contact with B6.1, the frequency of asymmetric centrosome behaviour appeared somewhat reduced with 2/8 E cells classed as asymmetric (Fig. 3D). Thus, contact with B6.1 is unlikely to play a critical role in the asymmetric centrosome behaviour of a neighbouring E cell. Ablation of an E cell also appeared to affect the centrosome behaviour of its contralateral neighbour. When one E cell at the early 24-cell stage was ablated, the frequency of asymmetric centrosome behaviour in the contralateral E cell appeared to decrease, with no migrations classed as asymmetric (0/7) (Fig. 3B and D). Altogether, we found no evidence to suggest that the asymmetric centrosome migration of the E cell was under the influence of a specific neighbouring cell. Rather, we suppose that ablation of neighbouring cells altered the E cell shape and that this change in E cell shape may be affecting the behaviour of the centrosomes. In order to test this possibility, we first measured the width of each E cell analysed in Fig. 3D and found that indeed, the cell ablations had an impact on the shape of E cells (Fig. 3E). Finally, we tested if there was a correlation between cell shape and centrosome migration angle (Fig. 3F). We found a moderate correlation between the centrosome migration angle and the width of the E cell, which was supported by statistical analysis ($r=-0.63$, $p<0.0001$). Thus, the narrower the E cell shape becomes, the more asymmetrically the two centrosomes tend to migrate.

We conclude that the asymmetric centrosome migration of E cells is influenced by cell shape. In the following sections, we analyse in detail the NN cell division.

2.3. NN cell spindle rotation requires both microtubules and actomyosin

The NN cell division is oriented by rotation of the mitotic spindle. In other systems, astral microtubules play a central role in controlling spindle orientations relative to cell shape and cortical cues (reviewed in Théry and Bornens, 2006; Morin and Bellaïche, 2011). Microfilaments (F-actin) are also implicated in spindle orientation and are thought to participate in the establishment of cellular polarity (reviewed in Nance and Zallen, 2011). In addition, F-actin may itself be an integral component of the cortical cues required to orient the spindle (Théry et al., 2005; Castanon et al., 2013). Our data show similarly that the NN cell spindle rotation is dependent on these cytoskeletal elements. The role of microtubules was addressed by observing ensconsin::3xGFP labelled spindles in embryos treated with a low dose of nocodazole (5 nM) from the beginning of the NN cell cycle. This dose was sufficient to reduce the size of asters but did not destroy the spindles, although spindles appeared somewhat smaller in size. This treatment resulted in inhibition of NN spindle rotation (Fig. 4). Similarly, treatment of embryos either with cytochalasin B, an inhibitor of actin filament polymerisation, or blebbistatin, an inhibitor of myosin II, prevented spindle rotation (Fig. 4). Thus, the spindle rotation of NN cells is dependent on an intact microtubule and actomyosin system, although these experiments did not allow us to discriminate whether the effects are cell autonomous or non-cell autonomous.

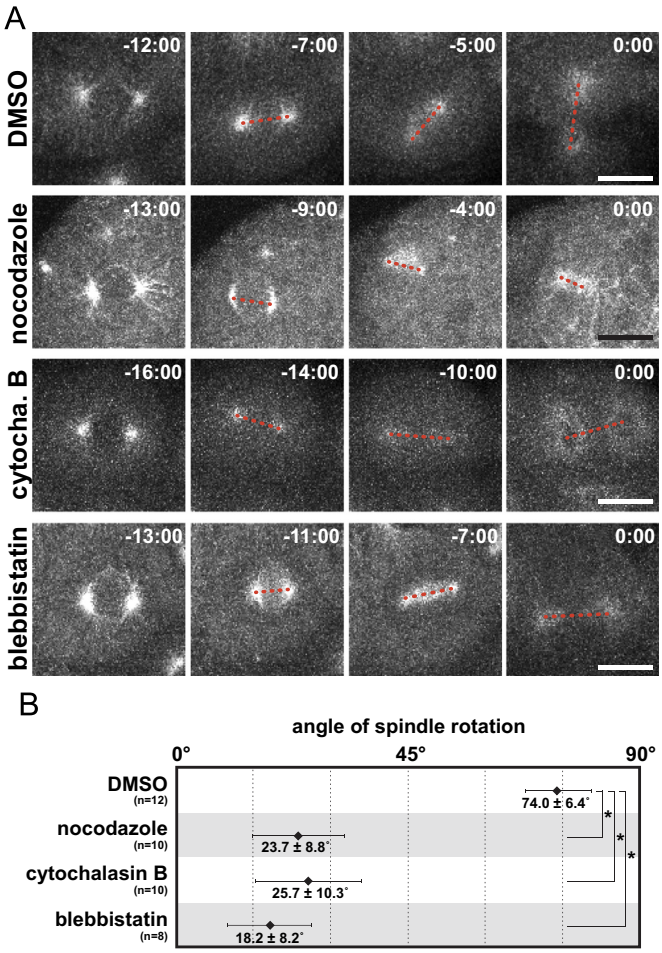

Fig. 4. Role of cytoskeletal elements in NN spindle rotation, Effects of DMSO (as control), nocodazole, cytochalasin B and blebbistatin on spindle rotation in NN cells. (A) Frames from confocal 4D movies of ensconsin::3xGFP-expressing embryos treated with the pharmacological inhibitors indicated on the left; nocodazole (5 nM), cytochalasin B (2.5 μg/ml) and blebbistatin (100 μM). Each frame corresponds a max intensity z-projection of selected sections. Red dotted lines correspond to the spindle axis. Animal pole side is up. Time is indicated as minutes: seconds with 0:00 corresponding to the onset of anaphase. Scale bars are 20 μm. (B) Quantification of the effect of inhibitor treatments on NN spindle rotation. Spindle rotation was measured as an angle corresponding to the difference in the spindle axes at the onset of metaphase compared to the onset of anaphase. Error bars show the standard deviation. *, $p<0.0001$ by unpaired t-test.

2.4. Cytoplasmic asymmetries associated with spindle rotation in NN cells

During the two successive cell divisions of the NNE and NN cells in *Phallusia mammillata*, mitochondria are differentially segregated, such that they accumulate in the animal pole side (marginal) cell (Zalokar and Sardet, 1984). We addressed when this cytoplasmic polarisation takes place relative to the NN cell spindle rotation by examining live embryos in which mitochondria were labelled with MitoTracker and microtubules were labelled with ensconsin::3xGFP. This analysis showed that the mitochondria, which initially localise around the nucleus (Figs. 5A, -9:00), start to segregate towards the animal pole at the onset of nuclear envelope break down (NEBD) (Figs. 5A, -7:00). By the time the mitotic spindle starts to rotate, the mitochondria have already formed a mass on the animal pole side (Figs. 5A, -5:00 time point; and

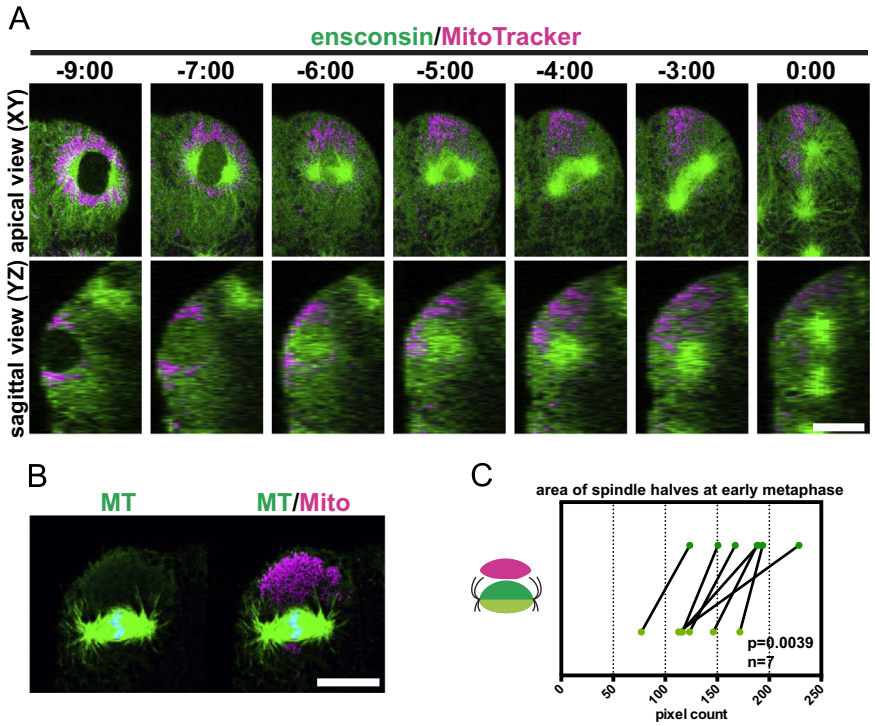

Fig. 5. Spindle asymmetry in NN cells. (A) Selected frames from confocal 4D image stacks of ensconsin::3xGFP-expressing embryos stained with MitoTracker. Each frame of XY view corresponds to a single z-plane at the indicated time point. Each corresponding frame of YZ view was reconstructed from the same 4D image data. Animal pole side is up and embryo midline to the left in the XY view. Time is indicated as minutes:seconds with 0:00 corresponding to the onset of anaphase. Scale bar corresponds to 20 μm. (B) Immunofluorescence images of NN cells labelled for microtubules (MT) and mitochondria (Mito) at early metaphase (corresponding to panel -6:00 in A). Each image is a single optical section. DNA was counterstained with DAPI. Animal pole side is up. Scale bar corresponds to 20 μm. (C) Quantification of the asymmetric shape of NN spindles at early metaphase. Graph shows the different size of early metaphase NN spindle halves on the mitochondria-side (dark green) compared to contra-mitochondria side (light green), measured from immunofluorescence images (in pixels) in individual NN cells. Drawing next to the graph shows a NN spindle with mitochondria mass in magenta and measured spindle halves in dark and light green. Total seven spindles were analysed: $p=0.0039$ (by paired t-test). Mean pixel sizes for the mitochondria- and contra-mitochondria-side halves are 177 (SD=33.8) and 123 (SD=29.5), respectively.

Movies 3 and 4). The astral microtubules of the rotating spindle penetrate the mitochondria mass. A sagittal view (YZ view) of NN cells reveals that mitochondria remain in the sub-apical area during both segregation and spindle rotation (Fig. 5A). Throughout the entire process, the nucleus and the spindle remain at a similar position relative to the apical contour of NN cells. In addition to the cytoplasmic asymmetry associated with mitochondria segregation in NN cells, we found that the spindle itself exhibits asymmetry (Fig. 5A). Soon after the spindle forms, it bulges on the side of the mitochondria mass (Figs. 5A, -5:00; Movies 3,4). As it rotates, the NN spindle takes on either a boomerang shape as in Fig. 5 A, -4:00 ($n=7/24$), or a form that bulged on the side of the mitochondria mass ($n=13/24$); such that 20 out of 24 rotating spindles exhibited clear asymmetry. In order to quantify the asymmetry of the metaphase spindle before rotation, we carried out immunostaining of mitochondria and microtubules (Fig. 5B). Max intensity projections of the spindles were divided into mitochondria and contra-mitochondria side halves and the area (in pixels) of each half was measured (Fig. 5C). In this analysis, all spindles examined ($n=7/7$) exhibited asymmetry with a clearly visible bulge on the side of the mitochondrial mass (Fig. 5C). The bulged form of NN spindles is also clearly visible in a 3D reconstruction of an NN cell immunostained for microtubules and mitochondria (Movie 5).

Thus, subcellular asymmetries precede spindle rotation in NN cells. The asymmetry of the spindle itself suggests the presence of a cytoplasmic microtubule-pulling force or stabilising activity on the side of the mitochondria mass.

2.5. *Microtubules and the actomyosin system are involved in distinct processes during NN cell cytoplasmic segregation and spindle rotation*

Both microtubules and the actomyosin system are required for the spindle rotation of NN cells (Fig. 4). We similarly addressed whether the segregation of mitochondria in NN cells depends on these cytoskeletal elements by observing spindle and mitochondria dynamics in embryos treated with cytochalasin B, blebbistatin or low doses of nocodazole. These treatments revealed that the segregation of mitochondria requires microfilaments and myosin activity but is not affected by treatment with low concentrations of nocodazole (Fig. 6A). Following nocodazole treatment, we also observed a pronounced displacement of the spindle, with its reduced microtubule asters, towards the mitochondria mass (Fig. 6B and C and Movie 6). Together with the structural asymmetries observed in the NN spindle (Fig. 5), this result supports the existence of a pulling force towards the mitochondria-enriched cytoplasmic domain. It also suggests that intact microtubules are required to maintain the spindle position at the centre of NN cell apical contour.

2.6. *Dynein is localised in the mitochondria-rich cytoplasmic domain in NN cells*

Our evidence for a microtubule-pulling force prompted us to address the potential involvement of dynein motor proteins during NN cell spindle rotation (reviewed in Morin and Bellaïche,

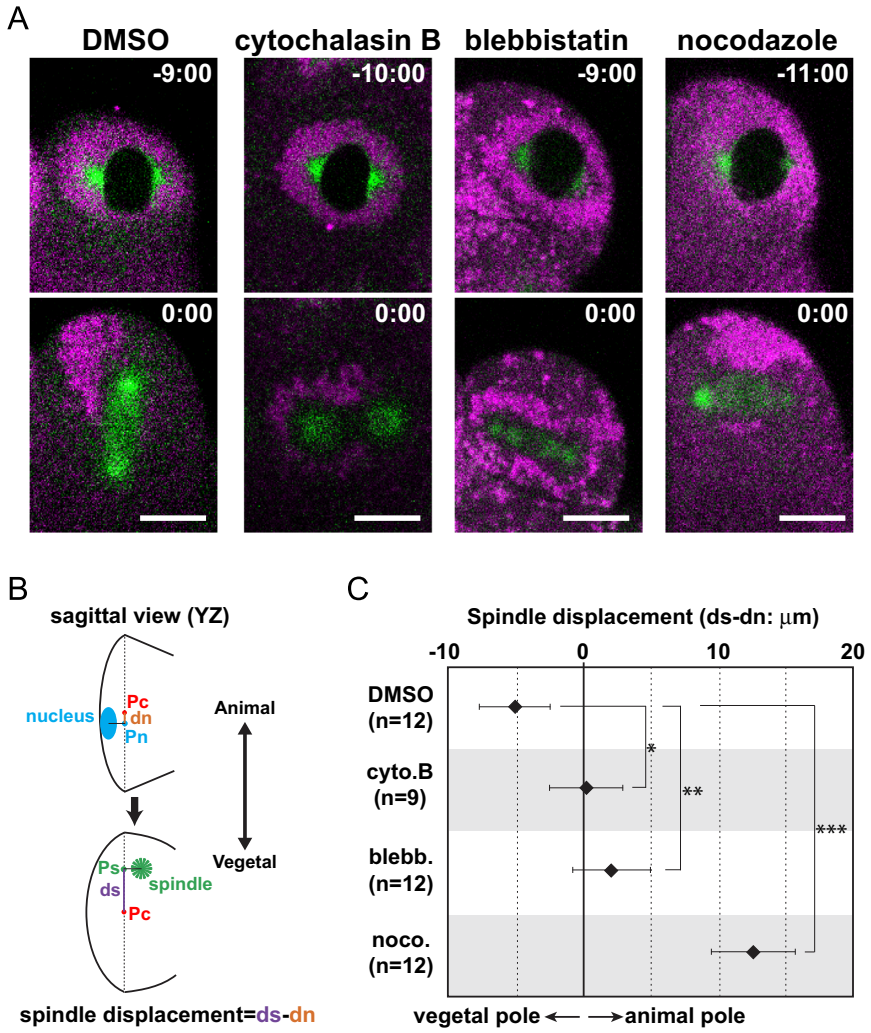

Fig. 6. Role of cytoskeletal elements for cellular polarity of NN cells. (A) The actomyosin system is required for segregation of mitochondria in NN cells. Panels show NN cells of embryos labelled for microtubules (green: ensconsin::3xGFP) and mitochondria (magenta: MitoTracker). Pharmacological inhibitors indicated above each panel were added to embryo culture when NN cells were at prophase; cytochalasin B (2.5 μg/ml), blebbistatin (100 μM) and nocodazole (5 nM). All embryos analysed exhibited the phenotype represented in the panels ($n=12$ for DMSO; $n=9$ for cytochalasin B; $n=12$ for blebbistatin; $n=12$ for nocodazole). Each image was extracted as a single z-plane from 4D image stacks. Animal pole side is up. The two time points shown correspond to prometaphase (upper) and the onset of anaphase (lower; set as 0:00). Scale bars are 20 μm. (B) Schematic drawings of NN cells in medial sagittal view showing how the displacement of NN spindles was measured. The upper drawing corresponds to NN cell at prometaphase, the lower drawing the onset of anaphase. The blue circle represents the nucleus while the green radial stripes represent a mitotic spindle that remains perpendicular to the A–V axis due to the lack of rotation in inhibitor-treated embryos. Dash lines connect the apical edges of the cell. Pc is the centre of the dashed line, representing the "centre of the cell". Pn and Ps represent the position of the prometaphase nucleus and the early anaphase spindle, respectively, projected onto the dashed line. The distances between Pc and Pn (dn) and between Pc and Ps (ds) were measured. (D) Quantification of the NN spindle displacement in embryos treated with cytoskeletal inhibitors. Graph shows the distance of the spindle displacement (ds–dn: in μm) in embryos treated with the inhibitors indicated on the left. When ds–dn is below zero, it means that the spindle was displaced in the vegetal pole direction. In DMSO-treated embryos, the middle of spindles was used to define Ps. Error bars indicate the standard deviation. *, $p<0.001$; **, $p<0.0001$; ***, $p<0.0001$ by unpaired t-test.

2011; Mitchison et al., 2012). We used two pharmacological inhibitors of dynein: ciliobrevin A, a small molecule inhibitor of the AAA+ ATPase motor cytoplasmic dynein (Firestone et al., 2012) and EHNA (erythro-9-[3-(2-hy-droxynonyl)]adenine) (Bouchard et al., 1981). Embryos were treated with ciliobrevin A or EHNA just after mitochondria segregation and just before spindle rotation started (Fig. 7A). Treatment with these dynein inhibitors blocked NN spindle rotation. Furthermore, spindle asymmetry was no longer visible in the majority of inhibitor-treated embryos (4/6 ciliobrevin A- and 7/8 EHNA-treated embryos no longer exhibited clear asymmetry). Next, we addressed the subcellular localisation of dynein in NN cells using double immunofluorescence visualisation of dynein (antibodies against the dynein heavy chain, DHC) and mitochondria (anti-HSP60). This revealed that dynein is enriched in similar, but broader, cytoplasmic domain to the mitochondria (Fig. 7B). While it remains to be shown which subcellular organelles dynein proteins associate with, our results support the hypothesis that a dynein-dependent pulling force from the mitochondria-rich cytoplasmic domain acts on the NN cell mitotic spindle.

2.7. Mitochondria segregation and spindle rotation take place in isolated NN cells

Finally, we tested if the cellular environment influences the spindle rotation of the NN cell. The cell division of NN cells is coupled with differential fate specification of the daughter cells. In *Ciona*, this fate specification is controlled by a cell contact-dependent directional ephrin signal (Picco et al., 2007). NN cells isolated at the beginning of their cell cycle undergo a symmetrical cell division in terms of the cell fate with both daughter cells adopting a notochord fate (Picco et al., 2007). In similarly-isolated

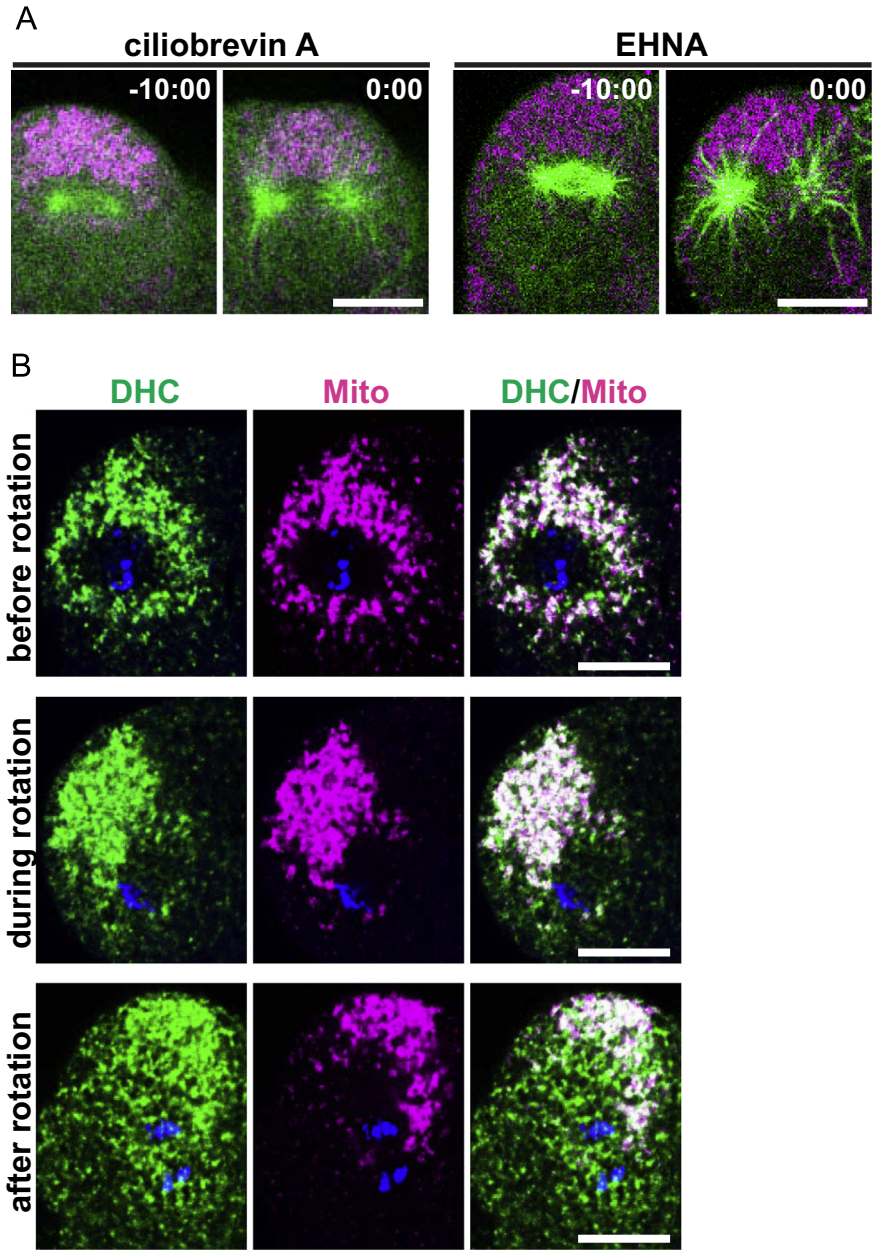

Fig. 7. Dynein is localised in the cytoplasmic domain enriched with mitochondria in NN cells. (A) Dynein protein function is required for spindle rotation in NN cells. Embryos were treated with ciliobrevin A or EHNA from the "decompaction" phase of 32-cell stage so that the mitochondria segregation had already taken place. Embryos were labelled for microtubules (green: ensconsin::3xGFP) and mitochondria (magenta: MitoTracker). Each image was extracted as a single z-plane from 4D image stacks. Animal pole side is up. Time is indicated as minutes:seconds with 0:00 corresponding to the onset of anaphase. Scale bars correspond to 20 μm. (B) Immunofluorescence images of NN cells labelled for dynein heavy chains (DHC) (green), mitochondria (magenta) and DNA (blue). Three phases of the spindle rotation, (top row) before spindle rotation, (middle row) during rotation and (bottom row) after rotation, were determined based on the alignment axis of chromosomes (blue). Animal pole side is up. Scale bars are 20 μm.

NN cells of *Phallusia*, the spindle still rotates, albeit with a reduced rotation angle ($57.8 \pm 11.8°$) compared to NN cells of intact embryos ($74.0 \pm 6.3°$) (Fig. 8A and B). Segregation of mitochondria also takes place in isolated NN cells with one spindle pole closely associated to the mitochondria mass ($n=6/7$) (Fig. 8A and Movie 7). This data suggest that the mitochondria segregation and the spindle rotation of NN cells can take place in the absence of cell–cell contacts, including the inductive signals that influence cell fate, as well as any physical constraints on the cell shape. However, it should be noted that the current experimental design did not allow us to determine whether the segregation and rotation took place along a specific axis.

3. Discussion

In this study, we analyse in detail the division of two sister cells, the NN and E cells, in the ascidian embryos of *Phallusia mammillata*. Both of these cells reorient their division axis, such that they divide along the same axis as their mother cell did. Our data provides evidence that the mitotic spindles of NN and E cells are oriented via distinct mechanisms. We propose the following model to describe the mechanisms of spindle orientation in these cells (Fig. 9). In the NN cell, the duplicated centrosomes arise on the animal pole side of the nucleus. The centrosomes migrate 90° in opposite directions such that the mitotic spindle forms orthogonal to the embryo midline (Fig. 1D). In this cell, cytoplasmic

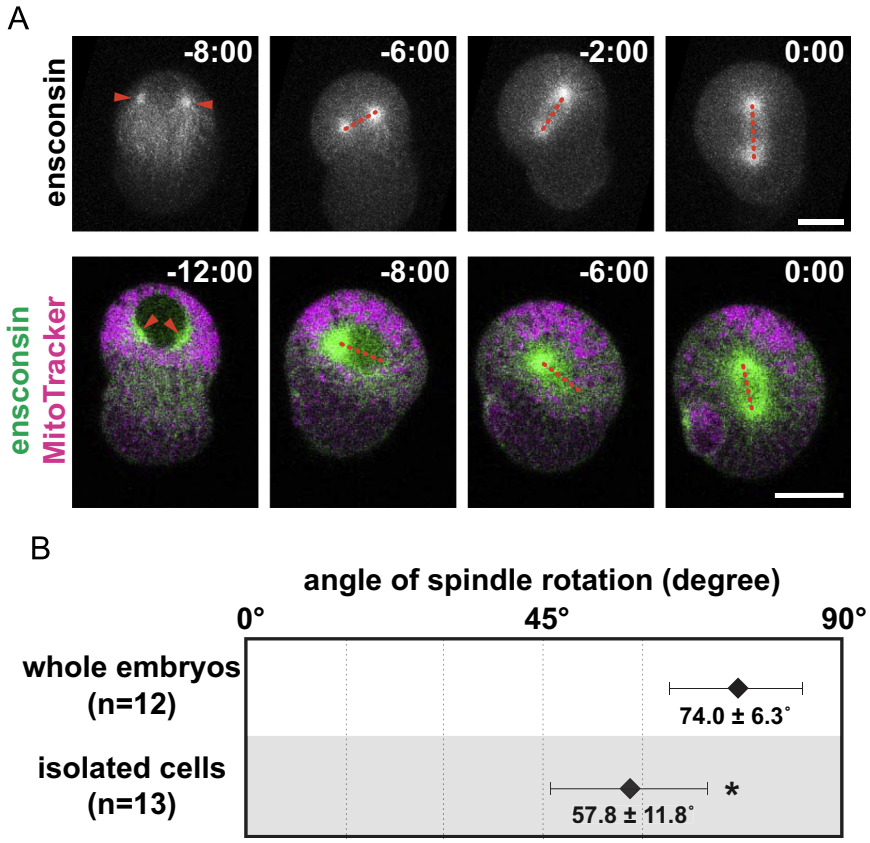

Fig. 8. Mitochondrial segregation and spindle rotation in isolated NN cells. (A) Selected frames from confocal 4D image stacks of isolated NN cells expressing ensconsin::3xGFP and stained with MitoTracker as indicated on the left of the panels. Frames in the top row are max intensity projections of selected planes while those in the bottom row are single z-planes. Red arrowheads and dotted lines indicate asters and spindle axes, respectively. Time is indicated as minutes:seconds with 0:00 corresponding to the onset of anaphase. Scale bars correspond to 20 μm. (B) The degree of spindle rotation in isolated NN cells was measured as an angle corresponding to the difference in the spindle axis prior to, and following, spindle rotation. Error bars show the standard deviation. *, $p < 0.01$ by unpaired *t*-test.

dynein and mitochondria, which are initially localised around the nucleus, displace towards the animal pole side of the cell in an actomyosin-dependent manner (Figs. 5, 6A and 7B). This displacement begins at the onset of NEBD and is completed by the time the mitotic spindle forms (Fig. 5A). We propose that this enrichment of cytoplasmic dynein exerts a net directional pulling force on both the polar and astral microtubules of the NN spindle, resulting in spindle asymmetry and rotation at metaphase. The elongated shape of the NN cell at metaphase may also contribute to the robust alignment of the mitotic spindle along the A–V axis, since spindle rotation is less pronounced in isolated cells compared to in intact embryos (Figs. 1C and 8). In the E cell, the duplicated centrosomes are positioned on the vegetal pole side of the nucleus (Fig. 1D). From the onset of the cell cycle, the E cell is

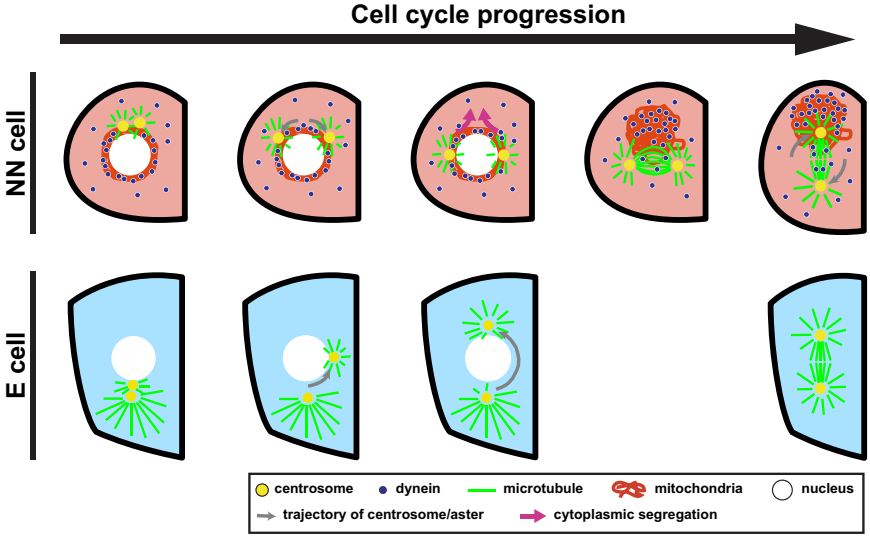

Fig. 9. Model proposing a mechanism for spindle orientation in NN and E cells Drawings depict NN and E cells from prometaphase to anaphase, following the code below. For each cell, animal pole side is at the top and embryo midline on the right. See text for details.

elongated along the A–V axis (Fig. 1C) and our data show a correlation between the elongated shape of the cell and the behaviour of the centrosomes (Fig. 3F). The duplicated centrosomes align along the A–V axis soon after their formation with the vegetal-side centrosome exhibiting a larger aster (Fig. 2B). While for the moment this remains entirely speculative, we propose that the cell cortex captures the astral microtubules of the distal aster, resulting in immobilisation of the distal centrosome. In contrast, the proximal centrosome, with its smaller aster, migrates around the nucleus towards the animal pole so that the mitotic spindle forms directly along the A–V axis (Fig. 1D).

3.1. NN cell spindle rotation and cytoplasmic displacement

Orientation of the NN cell division appears to begin with the enrichment of mitochondrial and dynein to the animal pole side of the cell, although it is currently unclear if there is any causal relationship between these two observations. We propose that this movement creates a net-asymmetric cytoplasmic pulling force. Mitochondria displacement and segregation also take place in the NN cells of *Ciona intestinalis* (Kobayashi et al., 2013) as well as in the NNE cell (mother cell of NN and E cells) in three solitary ascidian species, *Phallusia*, *Ciona* and *Halocynthia* (Zalokar and Sardet, 1984; Hudson et al., 2013; Takatori et al., 2010). In *Ciona* and *Halocynthia*, the segregation of mitochondria to the NN cell is accompanied by segregation of newly-synthesised zygotic transcripts (Hudson et al., 2013; Takatori et al., 2010). In *Halocynthia* NNE cells, mitochondria and zygotic transcripts are displaced in association with the nucleus and retained at the animal pole side in a Wnt5-dependent manner (Takatori et al., 2010). The mitotic spindle then migrates back to the centre of the apical contour just before initiation of cytokinesis. Nuclear migration and thus cytoplasmic segregation are microtubule-dependent (Takatori et al., 2010). In the NN cell division described here, however, the segregation of mitochondria and dynein appears to take place via a distinct mechanism. The nucleus and mitotic spindle of NN cells are not displaced towards the animal pole, but remain approximately at the centre of the apical contour (Fig. 6C). In addition, this cytoplasmic segregation is actomyosin-dependent but not affected by low doses of nocodazole. In both cases, the polarity cues directing cytoplasmic segregation remain unknown. Our ex-vivo experiment indicates that the mitochondria segregation in NN cells is a cell intrinsic property, although the experimental conditions used did not allow us to determine whether the segregation takes place along a specific axis.

While a causal link between the cytoplasmic concentration of mitochondria and dynein and the rotation of the NN cell spindle remains to be formally demonstrated, our data support the existence of dynein-dependent net-asymmetric pulling force from the cytoplasmic domain enriched with mitochondria. Asymmetry in the NN spindle itself suggests a microtubule pulling or stabilising force within the cytoplasm from the side of the mitochondrial mass (Fig. 5). Furthermore, the pronounced displacement of the spindle in nocodazole-treated embryos strongly suggests a pulling force towards the mitochondria side of the cell (Fig. 6). The preferential accumulation of dynein to the mitochondrial side of the cell, and the dependency of spindle rotation on dynein activity further support this hypothesis (Fig. 7). Co-immunodetection of mitochondria and dynein shows that dynein proteins follow similar temporal and spatial dynamics to mitochondria, although the two were not perfectly co-localised, suggesting that dynein proteins may (also) be associating with other organelles/structures (Fig. 7B). Motor proteins, including kinesin, dynein and myosin, are known to associate with intracellular organelles, including mitochondria, in eukaryotic cells and are important for transport of these organelles (reviewed in Rogers and Gelfand, 2000; Vale, 2003). In NN cells, the mitochondria-enriched cytoplasmic domain forms in an actomyosin-dependent manner and we propose that this cytoplasmic domain acts as a scaffold from which dynein exerts a pulling force onto both the astral and polar microtubules of the spindle. An organelle-mediated dynein-dependent cytoplasmic pulling force was shown to position the male pronucleus-centrosome complex in the centre of the *C. elegans* zygote, by exerting a net symmetric pulling force from evenly-distributed intracellular organelles, such as endosome, lysosome and yolk granule, onto the astral microtubules (Kimura and Kimura, 2011). However, our model for the NN cell division differs importantly from this since the cytoplasmic segregation would lead to a net-asymmetric pulling force.

The subcellular organisation of the mitochondria and dynein-rich cytoplasmic domain as well as the mechanisms of the cytoplasmic segregation itself remain to be addressed. In addition, questions remain concerning the mechanisms whereby the NN spindle rotates. It is not yet clear how the spindle remains central despite the net-asymmetric pulling force. The displacement of the spindle towards the mitochondria-rich side of the cell following treatment of embryos with low concentrations of nocodazole suggests that microtubules are involved (Fig. 6; Movie 6). Astral microtubules could be important in maintaining the central position of the spindle by mediating isotropic cytoplasmic pulling forces or by mediating compressive forces generated by astral microtubule buckling at the cortex (reviewed in Minc and Piel, 2013). In the case of NN cells, in which the cytoplasmic pulling force is asymmetrical, it is easier to envisage that astral microtubules are mediating isotropic compressive forces to counterbalance the directional cytoplasmic pulling force.

We also do not understand how the proposed directional cytoplasmic pulling force is converted into the rotational movement of the NN spindle. In order to convert pulling forces into torques in the context of spindle rotation, an imbalance in the pulling forces acting on two spindle poles is envisaged (reviewed in Morin and Bellaïche, 2011). For the NN cells, the mitotic spindle is first set perpendicular to the force-generating cytoplasmic domain situated on the animal pole side. Assuming that the cytoplasmic pulling force is proportional to the length of astral microtubules (Hamaguchi and Hiramoto, 1986; Minc et al., 2011), we propose two scenarios to account for the conversion of the cytoplasmic pulling force to a rotational movement. In the first, the two asters of NN spindle are similar in size and a slight tilt of the spindle axis relative to the axis of the pulling force generates the required imbalance. In the second, the two spindle poles exhibit distinct aster sizes, resulting in an imbalance in the pulling forces exerted on the poles. In either case, it remains a mystery how the spindles of a bilateral pair of NN cells have a tendency to rotate with bilateral symmetry (Fig. 2A).

3.2. Asymmetric centrosome migration in E cells

In contrast to the spindle rotation observed in NN cells, asymmetric centrosome migration results in the direct formation of the mitotic spindle along the A–V axis of E cells. A similar asymmetric centrosome migration has been shown in *Drosophila*, in male germline stem cells (mGSCs) (Yamashita et al., 2003) and in both larval and embryonic neuroblasts (NBs) (Rebollo et al., 2007; 2009). In the cell divisions described in *Drosophila*, the centrosome exhibiting a larger aster associates with cortical polarity cues, such as a contact site with the stem cell niche (mGSCs) or the apical cortex (NBs), and becomes immobilised. Importantly, in the cell division of mGSCs and NBs, there is a strong correlation between centrosome age and behaviour, such that the mother centrosome becomes immotile in mGSCs and the daughter centrosome becomes immotile in NBs (Yamashita et al., 2007; Conduit

and Raff, 2010; Januschke et al., 2011). In E cells, the centrosome with a larger aster becomes immotile, similar to the examples in *Drosophila*, although we were unable to distinguish mother from daughter centrosomes in our experiments. One notable feature of the E cell centrosome behaviour is that the centrosome duplication appears to take place along the A–V axis of the cell, resulting in an alignment of the nucleus and two centrosomes along the axis. The larger distal (vegetal-side) centrosome becomes immobilised (Fig. 2D). We propose a model in which the larger size of the distal aster, together with the elongated shape of the E cell, may facilitate the capturing of the distal aster by the E cell cortex, resulting in its immobilisation (Fig. 9).

In conclusion, we analysed in detail the division of a pair of embryonic sister cells in ascidian embryos. Our data are consistent with our proposed model whereby: (1) in E cells a cell shape-dependent mechanism directs asymmetric centrosome migration; (2) in NN cells a dynein-enriched cytoplasmic domain generates a net-asymmetric pulling force that leads to spindle rotation. It will be imperative in future study to address the molecular mechanisms controlling these oriented cell divisions. Additional works focusing on diverse cellular and developmental contexts are needed to understand the diversity of mechanisms that may control oriented cell division.

4. Materials and methods

4.1. Phallusia Embryos

Adult *Phallusia mammillata* were collected at Sète (Etang de Tau, Mediterranean coast, France). Embryo culture, cell isolation, cell ablation and microinjection are previously described (Sardet et al., 2011). Ensconsin::3xGFP and EB3::GFP RNA were synthesised from pRN3 plasmid (Lemaire et al., 1995) using T3 mMESSAGEmMACHINE kit (Life Technologies), and injected at 2 μg/μl into unfertilised eggs. The cDNA encoding EB3::GFP was a gift from Dr A. Akhmanova. FM4-64 (Molecular Probes) was used at 20 μg/ml to observe cell membranes. Embryos were treated with 1 μM Mitotracker Red 580 (Molecular Probes) for 20 min to label mitochondria.

4.2. Pharmacological inhibitors

DMSO (Sigma), as control, was diluted 1:1000. Nocodazole (Sigma), cytochalasin B (Sigma) and blebbistatin (Sigma) were used at 5 nM, 2.5 μg/ml and 100 μM, respectively. Embryos were treated with inhibitors from the onset of the 32-cell stage. To block dynein function after mitochondrial segregation at the 32-cell stage, embryos were treated with ciliobrevin A or EHNA when vegetal cells started to show “decompaction” (Nakatani and Nishida, 1994). ciliobrevin A (Sigma; as HPI-4) was used at 50 μM and EHNA (erythro-9-(2-Hydroxy-3-nonyl) adenine hydrochloride) (Tocris Biocience) at 0.5 mM. All stocks of inhibitors, with the exception of cytochalasin B and EHNA, were prepared in DMSO and diluted to at least 1:1000 in seawater. The stocks of cytochalasin B and EHNA were prepared in ethanol and diluted to 1:1000 and 1:100 in seawater.

4.3. Immunostaining

For microtubule immunostaining, embryos were fixed in cold methanol overnight and washed with PBS containing 0.1 % Triton-X (PBSTr). DM1A (Abcam) was diluted 1:100 in PBSTr containing 1 % BSA (BSA/PBSTr). Alexa Fluor 594 Goat Anti-Mouse IgG (Molecular Probes) was diluted 1:200 in BSA/PBSTr. For co-immunostaining of microtubules and mitochondria, anti-HSP60 antibody (Chenevert et al., 2013) and Alexa Fluor 488 Goat Anti-Rabbit IgG (Molecular Probes) were added at 1:50 and 1:200 dilution to the primary and secondary antibody reactions, respectively. For immunostaining of dynein heavy chains, embryos were fixed in artificial seawater containing 4% PFA overnight at 4 °C and then washed with PBSTr. Dynein HC antibodies (R-325) (Santa Cruz Biotechnology) were diluted at 1:50 in BSA/PBSTr. As secondary antibody, the MaxPO system (Nichirei Bioscience) was used at a dilution of 1:20 and signals were amplified using a TSA system, as described previously (Hudson et al., 2013). For co-immunostaining of mitochondria and dynein heavy chains, NN18 (ICN) (Chenevert et al., 2013) and Alexa Fluor 488 Goat Anti-Mouse IgG (Molecular Probes) were added at 1:50 and 1:200 dilutions, respectively. Immunostained embryos were mounted with VECTASHIELD Mounting Medium with DAPI (Vector Laboratories).

4.4. Imaging and quantification

Images of fixed samples and time-lapse movies of live samples were acquired using a Leica SP5 confocal microscope system with a Leica HCX PL APO 40x/1.3NA objective lens (Negishi et al., 2013). DIC time-lapse movies were acquired with a Zeiss Axiovert 200 microscope with a Zeiss plan achromat 40 × /0.95NA objective lens operated using MetaMorph software (Universal Imaging Cooperation). For all image acquisitions, embryos were titled so that the apical contour of NN or E cells was as parallel as possible to the imaging plane with the embryonic median plane perpendicular to the coverslip (Negishi et al., 2013). All image processing and analyses were conducted using ImageJ software (National Institutes of Health). All statistical analyses were conducted using GraphPad Prism 6 software (GraphPad Software).

For all image analyses, if necessary, image stacks were reoriented so that the apical contour faces parallel to the screen. To quantify the cell shape of NN and E cells (Fig. 1B and C), we measured the length and width of their apical contour based on 4D image stacks of embryos labelled for microtubules (ensconsin::3xGFPs) and membrane (FM4-64) (Fig. 1B). For the length, we measured the line that is parallel to the embryonic midline and crosses the centre of the nucleus or of the spindle. For the width, the line that is perpendicular to the length and crosses the centre of the nucleus or of the spindle was measured.

To quantify the size difference of two asters in E cells (Fig. 2B and D), 3D image stacks of embryo immunostained for microtubules were converted into binary images and the size of the asters, in pixel counts, in each z-section was measured.

To quantify the degree of the asymmetry of centrosome migration in E cells (Fig. 3D), we measured the angle of two lines crossing the centre of the nucleus (Fig. 3C). The first line is from the site in which centrosome duplication took place to the centre of the nucleus, while the second line joins the positions of the two centrosomes when migration is complete. In this quantification system, 90° would indicate that two centrosomes migrated equal distance, thus the centrosome migration was symmetrical, whereas 180° would indicate complete asymmetric migration. For this quantification, we selected two time points, at the beginning and end of centrosome migration, from 4D image stacks of ensconsin::3xGFPs-expressing embryos. If necessary, 4D image stacks were first reoriented so that the apical contour of the cell faced parallel to the screen.

To quantify the width of E cells (Fig. 3E), we measured the line perpendicular to the embryonic midline crossing the centre of nucleus as in Fig. 1B.

To quantify the degree of spindle rotation in NN cells (Figs. 4B and 8B), an angle corresponding to the difference in the spindle axes at the onset of metaphase and at the onset of anaphase was measured based on corresponding 3D stacks selected from 4D

image data of embryos expressing ensconsin::3xGFPs.

To quantify the area of mitochondria side half and contra-mitochondria side half of NN spindles (Fig. 5C), 3D image stacks of embryos immunostained for microtubules were analysed as follows. Using max intensity projection, 3D stacks were then projected into 2D images, which were subsequently converted into binary images. The number of pixels covering mitochondria side half and contra-mitochondria side half of NN spindles was counted as the area representing the NN spindle halves.

To quantify the distance of the displacement of NN spindles in the animal pole direction following treatment of cytoskeletal inhibitors (Fig. 6B and C), first the 4D image stacks of ensconsin::3xGFPs-expressing embryos were reoriented so that the embryonic midline run vertically. YZ-view images were then reconstructed from selected 4D image stacks. In these YZ images, the cell centre (Pc) was defined at the midpoint of the line connecting the two apical edges (Fig. 6B). In order to define the position of the prometaphase nucleus, Pn, the nucleus centre was projected onto the apical-edge line at a right angle (Fig. 6B). The spindle position at the onset of anaphase, Ps, was defined in the same manner as for Pn. The distances between Pc and Pn (dn) and between Pc and Ps (ds) were measured in order to quantify the relative position of these organelles along the A–V axis of NN cells. The animal side of the apical centre was measured with positive numbers and the vegetal side with negative numbers. The distance of the spindle displacement was obtained by subtracting dn from ds (ds–dn). All dn values were within $\pm 3.2\,\mu m$ of the cell centre at prometaphase.

Acknowledgements

We thank Clare Hudson, Cathy Sirour and Evelyn Houliston for helpful discussions and comments on the manuscripts, Alex McDougall and members of his group for assistance with *Phallusia*, Janet Chenevert for providing anti-HSP60 and NN18 antibodies and Laurent Gilletta and Sophie Collet for animal husbandry. TN was a recipient of a postdoc fellowship from the Agence Nationale de la Recherche. HY is a CNRS investigator. The current study was supported by the CNRS, the Université Pierre et Marie Curie, the ARC (1144) and the Agence Nationale de la Recherche (ANR-09-BLAN-0013-01).

References

Bouchard, P., Penningroth, S.M., Cheung, A., Gagnon, C., Bardin, C.W., 1981. Erythro-9-[3-(2-Hydroxynonyl)]adenine is an inhibitor of sperm motility that blocks dynein ATPase and protein carboxylmethylase activities. Proc. Natl. Acad. Sci. USA 78, 1033–1036.

Castanon, I., Abrami, L., Holtzer, L., Heisenberg, C.P., van der Goot, F.G., González-Gaitán, M., 2013. Anthrax toxin receptor 2a controls mitotic spindle positioning. Nat. Cell Biol. 15, 28–39.

Chenevert, J., Pruliere, G., Ishii, H., Sardet, C., Nishikata, T., 2013. Purification of mitochondrial proteins HSP60 and ATP synthase from ascidian eggs: implications for antibody specificity. PLoS One 8, e52996. http://dx.doi.org/10.1371/journal.pone.0052996.

Conklin, E., 1905. The organization and cell lineage of the ascidian egg. J. Acad. Nat. Sci. (Phila.) 13, 1–119.

Conduit, P.T., Raff., J.W., 2010. Cnn dynamics drive centrosome size asymmetry to ensure daughter centriole retention in Drosophila neuroblasts. Curr. Biol. 20, 2187–2192.

Conrad, G.W., Rappaport, R., 1981. Mechanism of cytokinesis in animal cells. In: Zimmerman, A., Forer, A. (Eds.), Mitosis/Cytokinesis. Academic Press, New York, pp. 365–396.

Delsuc, F., Brinkmann, H., Chourrout, D., Philippe, H., 2006. Tunicates and not cephalochordates are the closest living relatives of vertebrates. Nature 439, 965–968.

Firestone, A.J., Weinger, J.S., Maldonado, M., Barlan, K., Langston, L.D., O'Donnell, M., Gelfand, V.I., Kapoor, T.M., Chen, J.K., 2012. Small-molecule inhibitors of the AAA+ ATPase motor cytoplasmic dynein. Nature 484, 125–129.

Freeman, G., 1983. The role of egg and organization in the generation of cleavage patterns. In: Jeffery, W.R., Raff, R.A. (Eds.), Time, Space, and Pattern in Embryonic Development. Alan R. Liss, Inc., New York, pp. 171–196.

Hamaguchi, M.S., Hiramoto, Y., 1986. Analysis of the role of astral rays in pronuclear migration in sand dollar eggs by the colcemid-UV method. Dev. Growth Differ. 28, 143–156.

Hudson, C., Kawai, N., Negishi, T., Yasuo, H., 2013. β-Catenin-driven binary fate specification segregates germ layers in ascidian embryos. Curr. Biol. 23, 491–495.

Januschke, J., Llamazares, S., Reina, J., Gonzalez, C., 2011. *Drosophila* neuroblasts retain the daughter centrosome. Nat. Commun . http://dx.doi.org/10.1038/ncomms1245.

Kim, G.J., Kumano, G., Nishida, H., 2007. Cell fate polarization in ascidian mesenchyme/muscle precursors by directed FGF signaling and role for an additional ectodermal FGF antagonizing signal in notochord/nerve cord precursors. Development 134, 1509–1518.

Kimura, K., Kimura, A., 2011. Intracellular organelles mediate cytoplasmic pulling force for centrosome centration in the *Caenorhabditis elegans* early embryo. Proc. Natl. Acad. Sci. USA 108, 137–142.

Kiyomitsu, T., Cheeseman, I.M., 2012. Chromosome- and spindle-pole-derived signals generate an intrinsic code for spindle position and orientation. Nat. Cell Biol. 14, 311–317.

Kobayashi, K., Yamada, L., Satou, Y., Satoh, N., 2013. Differential gene expression in notochord and nerve cord fate segregation in the *Ciona intestinalis* embryo. Genesis 51, 647–659.

Lechler, T., Fuchs, E., 2005. Asymmetric cell divisions promote stratification and differentiation of mammalian skin. Nature 437, 275–280.

Lemaire, P., Garrett, N., Gurdon, J.B., 1995. Expression cloning of *Siamois*, a *Xenopus* homeobox gene expressed in dorsal-vegetal cells of blastulae and able to induce a complete secondary axis. Cell 81, 85–94.

Lemaire, P., Smith, W.C., Nishida, H., 2008. Ascidians and the plasticity of the chordate developmental program. Curr. Biol. 18, R620–R631.

Minc, N., Burgess, D., Chang, F., 2011. Influence of cell geometry on division-plane positioning. Cell 144, 414–426.

Minc., N., Piel., M., 2013. Anthrax receptors position the spindle. Nat. Cell Biol. 15 (1), 11–13.

Minokawa, T., Yagi, K., Makabe, K.W., Nishida, H., 2001. Binary specification of nerve cord and notochord cell fates in ascidian embryos. Development 128, 2007–2017.

Mitchison, T., Wühr, M., Nguyen, P., Ishihara, K., Groen, A., Field, C.M., 2012. Growth, interaction, and positioning of microtubule asters in extremely large vertebrate embryo cells. Cytoskeleton 69, 738–750.

Morin, X., Bellaïche, Y., 2011. Mitotic spindle orientation in asymmetric and symmetric cell divisions during animal development. Dev. Cell 21, 102–119.

Nakatani, Y., Nishida, H., 1994. Induction of notochord during ascidian embryogenesis. Dev. Biol. 166, 289–299.

Nance, J., Zallen, J.A., 2011. Elaborating polarity: PAR proteins and the cytoskeleton. Development 138, 799–809.

Negishi, T., McDougall, A., Yasuo, H., 2013. Practical tips for imaging ascidian embryos. Dev. Growth Differ. 55, 446–453.

Peyre, E., Jaouen, F., Saadaoui, L., Haren, A., Merdes, P., Durbec, X. Morin, X., 2011. A lateral belt of cortical LGN and NuMA guides mitotic spindle movements and planar division in neuroepithelial cells. J. Cell Biol. 193, 141–154.

Picco, V., Hudson, C., Yasuo H., H., 2007. Ephrin-Eph signalling drives the asymmetric division of notochord/neural precursors in *Ciona* embryos. Development 134, 1491–1497.

Prodon, F., Chenevert, J., Hébras, C., Dumollard, R., Faure, E., Gonzalez-Garcia, J., Nishida, H., Sardet, C., McDougall, A., 2010. Dual mechanism controls asymmetric spindle position in ascidian germ cell precursors. Development 137, 2011–2021.

Rebollo, E., Roldán, M., Gonzalez, C., 2009. Spindle alignment is achieved without rotation after the first cell cycle in *Drosophila* embryonic neuroblasts. Development 136, 3393–3397.

Rebollo, E., Sampaio, P., Januschke, J., Llamazares, S., Varmark, H., González., C., 2007. Functionally unequal centrosomes drive spindle orientation in asymmetrically dividing *Drosophila* neural stem cells. Dev. Cell 12 (3), 467–474.

Rogers, S.L., Gelfand., V.I., 2000. Membrane trafficking, organelle transport, and the cytoskeleton. Curr. Opin. Cell Biol. 12 (1), 57–62.

Sardet, C., McDougall, A., Yasuo, H., Chenevert, J., Pruliere, G., Dumollard, R., Hudson, C., Hebras, C., Le Nguyen, N., Paix, A., 2011. Embryological methods in ascidians: the Villefranche-sur-Mer protocols. Methods Mol. Biol. 770, 365–400.

Satoh, N., Rokhsar, D., Nishikawa, T., 2014. Chordate evolution and the three-phylum system. Proc. Biol. Sci. 281, 20141729.

Strome, S., 1993. Determination of cleavage planes. Cell 72, 3–6.

Takatori, N., Kumano, G., Saiga, H., Nishida, H., 2010. Segregation of germ layer fates by nuclear migration-dependent localization of *Not* mRNA. Dev. Cell 19, 589–598.

Théry, M., Bornens, M., 2006. Cell shape and cell division. Curr. Opin. Cell Biol. 18, 648–657.

Théry, M., Racine, V., Pépin, A., Piel, M., Chen, Y., Sibarita, J.B., Bornens, M., 2005. The extracellular matrix guides the orientation of the cell division axis. Nat. Cell Biol. 7, 947–953.

Vale, R.D., 2003. Myosin V motor proteins: marching stepwise towards a mechanism. J. Cell Biol. 163 (3), 445–450.

Vienne, A., Pontarotti, P., 2006. Metaphylogeny of 82 gene families sheds a new

light on chordate evolution. Int. J. Biol. Sci. 2, 32–37.
von Dassow, G., Verbrugghe, K.J., Miller, A.L., Sider, J.R., Bement, W.M., 2009. Action at a distance during cytokinesis. J. Cell Biol. 187, 831–845.
Wilson, E.B., 1925. Growth, cell division and development. In: Wilson, E.B. (Ed.), The Cell in Development and Heredity. The Macmillan Company, New York, pp. 361–395.
Yamashita, Y.M., Mahowald, A.P., Perlin, J.R., Fuller, M.T., 2007. Asymmetric inheritance of mother versus daughter centrosome in stem cell division. Science 315, 518–521.
Yamashita, Y.M., Jones, D.L., Fuller, M.T., 2003. Orientation of asymmetric stem cell division by the APC tumor suppressor and centrosome. Science 301, 1547–1550.
Zalokar, M., Sardet, C., 1984. Tracing of cell lineage in embryonic development of *Phallusia mammillata* (Ascidia) by vital staining of mitochondria. Dev. Biol. 102, 195–205.
Zheng, Z., Zhu, H., Wan, Q., Liu, J., Xiao, Z., Siderovski, D.P., Du, Q., 2010. LGN regulates mitotic spindle orientation during epithelial morphogenesis. J. Cell Biol. 189, 275–288.